

RESEARCH ARTICLE

Life in the flow: unique adaptations for feeding on drifting zooplankton in garden eels

Alexandra Khrizman^{1,2,*}, Gal Ribak³, Dmitri Churilov¹, Irena Kolesnikov¹ and Amatzia Genin^{1,4}

ABSTRACT

A major challenge faced by sessile animals that feed in the flow is to maintain effective feeding postures while enduring hydrodynamic forces. Garden eels exhibit an exceptional lifestyle: feeding on drifting zooplankton while being ‘anchored’ in a burrow they dig in the sand. Using underwater observations, sampling and three-dimensional video recording, we measured the feeding rates and characterized feeding postures of garden eels under a wide range of current speeds. We show that the eels behaviorally resolve the trade-off between adverse biomechanical forces and beneficial fluxes of food by modulating their body postures according to current speeds. In doing so, the eels substantially reduce drag forces when currents are strong, yet keep their head well above bottom in order to effectively feed under conditions of high prey fluxes. These abilities have allowed garden eels to become one of the rare oceanic fishes that live in sandy, predation-rich habitats and feed on zooplankton while being attached to the bottom.

KEY WORDS: Fish, *Gorgasia sillneri*, Biomechanics, Drag force, Zooplanktivory

INTRODUCTION

Marine sessile organisms depend on currents for the delivery and replenishment of suspended and dissolved commodities, such as plankton, oxygen and nutrients (Hamner et al., 1988; Baynes and Szmant, 1989; Harris, 1990). However, water motion exerts hydrodynamic forces that intensify with velocity and acceleration, creating physical stresses that could potentially dislodge an organism or hinder its basic functions (e.g. Koehl and Wainwright, 1977; Seymour et al., 1989). Therefore, organisms living in the flow should be adapted to sustain these stresses. Indeed, a large variety of adaptations have been documented (Vogel, 1994), such as small body size in exposed intertidal habitats (Denny et al., 1985; Carrington, 1990), flow-induced modulations of body shape (Koehl, 1977, 1982; Koehl and Alberte, 1988; Armstrong, 1989; Johnson and Koehl, 1994) and changes in body tenacity or skeletal strength (Bell and Gosline, 1997; Chang et al., 2007). Additionally, adaptations to reduce drag forces during strong currents were observed among

individuals living in habitats with variations in flow velocities, including flexible bending (Koehl and Wainwright, 1977; Holbrook et al., 1991; Gaylord and Denny, 1997; Denny and Gaylord, 2002; Sand-Jensen, 2003; Stewart, 2004; Boller and Carrington, 2006), reorientation (Best, 1988; Vogel, 1994) and passive or active modulation of body shape (Koehl, 1977, 1982; Armstrong, 1989; Carrington, 1990; Harder et al., 2004; Boller and Carrington, 2006). Although an adaptation that avoids being dislodged may be sufficient for autotrophic organisms, for planktivorous organisms, the adaptation should also account for the fact that modulation of body shape can greatly interfere with feeding (Okamura and Partridge, 1999).

Although sessility is quite common among marine invertebrates, a sessile lifestyle is rare in vertebrates (e.g. larval lampreys; Docker, 2014). An outstanding example is found in the sub-family of garden eels (Heterocongrinae) – elongated fish that feed on drifting zooplankton while being anchored to the bottom (Movie 1; Fig. 1). Similar to other site-attached planktivorous fish (Kiflawi and Genin, 1997), garden eels depend on the flow for food delivery. However, unlike ‘free’ fish, which can freely swim to strike their prey, garden eels ‘anchor’ themselves to the bottom by keeping their posterior body section inside a burrow they dig in the sand. They strike zooplankton by maneuvering the upper body, which remains outside the burrow during foraging. The burrow is used as shelter where the eel retreats at times of danger and where it remains during the night (Böhlke, 1957; Fricke, 1969, 1970; Clark, 1980).

A physical–biological trade-off is inherent to this lifestyle, as stronger currents exert higher drag forces at times when food fluxes are higher. Therefore, passive bending under strong currents should be avoided as it may hinder feeding when food supply is high. A solution through which drag forces would be reduced under strong currents while allowing the animal to continue feeding would therefore be beneficial. The main objectives of this study were to quantify the eels’ *in situ* feeding rates and examine the ways the eels resolve the aforementioned trade-off. Based on the observations of the flow-dependent changes in the eels’ feeding postures (Fig. 1), we hypothesized that garden eels’ postures at higher current speeds are a compromise between the need to minimize the hydrodynamic forces acting on the body and the need to retain feeding when food fluxes are high. Although the postural changes in garden eels have been reported before (Fricke, 1969, 1970), they were neither quantitatively measured nor were their adaptive benefits assessed.


MATERIALS AND METHODS

Study species

The garden eel *Gorgasia sillneri* Klausewitz 1962 is common in the Red Sea, where it lives in large colonies (Fig. 1) consisting of hundreds to a few thousands of individuals (Clark, 1980). Colonies are usually found adjacent to or inside seagrass meadows, at depths of 4–55 m (Fricke, 1969, 1970; Clark, 1980). The eels reside in sinusoidal burrows they dig in the sand, the length of which is slightly longer than their body, and 6–16 mm in diameter (Fricke,

¹The Interuniversity Institute for Marine Sciences in Eilat, Eilat 88103, Israel. ²The Fredy and Nadine Hermann Institute of Earth Sciences, Hebrew University of Jerusalem, Jerusalem 91904, Israel. ³School of Zoology, Faculty of Life Sciences, Tel Aviv University, Tel Aviv 69978, Israel. ⁴Department of Ecology, Evolution, and Behavior, Alexander Silberman Institute of Life Sciences, Hebrew University of Jerusalem, Jerusalem 91904, Israel.

*Author for correspondence (alexey.khrizman@mail.huji.ac.il)

 A.K., 0000-0001-9052-0154; G.R., 0000-0002-6267-5471; A.G., 0000-0001-8239-8902

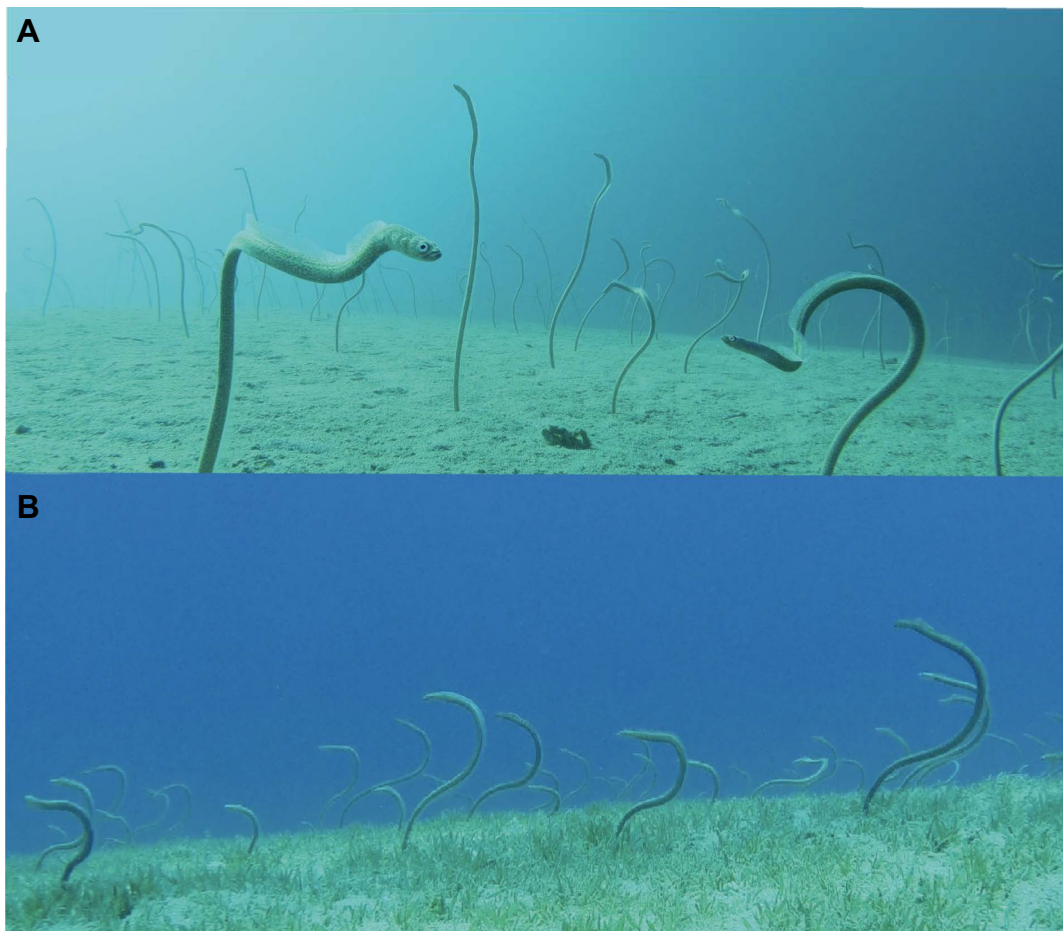


Fig. 1. A colony of garden eels of the species *Gorgasia sillneri*. The colony is at 6 m depth in the northern Gulf of Eilat (Aqaba), Red Sea, under conditions of (A) weak (4 cm s^{-1}) and (B) strong (26 cm s^{-1}) currents.

1969, 1970; Clark, 1980; Tyler and Smith, 1992). The males reach 75–95 cm in total length while females are 55–75 cm long (Clark, 1980). The cross-section of the eels' body is nearly circular (Klausewitz, 1962). The pectoral fins are small, and the dorsal fin extends along most of the body (Klausewitz, 1962), similar in width to the body diameter.

Several studies on the ecology, behavior and morphology of *G. sillneri* were carried out in the Red Sea a few decades ago (e.g. Fricke, 1969, 1970, 1971; Clark, 1980; Clark et al., 1990).

Study site

Our work was carried out at 6–10 m depth at two sites in the northern Gulf of Aqaba, Red Sea ($29^{\circ}36'N$, $34^{\circ}56'E$) (Fig. S1). A detailed description of the local reef and its environmental conditions can be found in Reiss and Hottinger (1984), Yahel et al. (2002) and Genin et al. (2009). Both sites are exposed to semidiurnal tidal currents (Monismith and Genin, 2004) with a dominance of long-shore velocities with an average speed of $\sim 10 \text{ cm s}^{-1}$ and maximum values around 50 cm s^{-1} (Genin and Paldor, 1998).

Data collection

In order to reconstruct the eels' body postures in three dimensions (3D), we used two underwater video cameras (GoPro Hero 3+ black; resolution 2704×1524 pixels; frame rate of $29.97 \text{ frames s}^{-1}$; medium field of view) mounted 1.8 m apart on a frame positioned

on the seafloor $\sim 0.2 \text{ m}$ above the bottom (Fig. S2). In each recording session, prior to data acquisition, the cameras were calibrated for 3D processing using a wand with two bright points 10 cm apart, by slowly waving the wand in front of the cameras across the entire field of view. After calibration, the foraging garden eels were recorded for at least 40 min (hereafter a 'session'). The two cameras were synchronized (to within a single frame) using an abrupt sound cue every 10 min. Current speed and direction were measured using a current profiler (Aquadopp 2 MHz, Nortek AS, Rud, Norway), placed a few meters away from the cameras. For this study we used the Aquadopp's lower range (0.2–1.0 m above bottom), corresponding to the height of the eels above bottom during foraging. Current measurements, recorded at 1 Hz, were averaged over 2 min intervals for the entire duration of the camera records. The data were collected at varying times of the day during a total of 11 separate sessions between 16 February 2015 and 26 December 2016 (Table S1).

Camera calibration

The first step in the data processing for each session was to calibrate the cameras in order to transform the 2D camera coordinates (u, v pixels) into 3D coordinates (XYZ system). This was done based on intrinsic (camera and depth dependent) and extrinsic (position dependent) calibrations of the cameras. The intrinsic parameters were obtained at the start of the study by recording a checkerboard (8×8 squares, $3.7 \times 3.7 \text{ cm}$ each) from 87 angles at the depth from which all recording

sessions were later taken, processed using the Camera Calibration Toolbox for MATLAB (http://www.vision.caltech.edu/bouguetj/calib_doc). The extrinsic parameters were obtained for each session with DLTdv5 code (Hedrick, 2008), using at least 350 frames in which the two points on the wand were clearly visible in the two cameras. Using easyWand5 code (Theriault et al., 2014), the u, v coordinates of the circles in both of the videos were transformed into an XYZ Cartesian world coordinate system, taking into account the distance between the circles (10 cm) and the distortion coefficients of the cameras obtained from the checkerboard calibration. An additional 150 frames were then used for each session to produce an estimate of the bias and the error in our determination of the XYZ position at a confidence interval of 98%. We ensured the bias was always $<0.5\%$ and the error was always $<5\%$ (except a single session in which the bias was 0.6% and a separate session with an error of 6.4%).

Data analysis

In order to reconstruct the body posture of an eel, we digitized the 3D positions of 15–35 points along the body using DLTdv5 (Hedrick, 2008). The number of points digitized per eel was a function of its body curvature and length, with fewer points digitized across linear sections. Linear interpolation between neighboring digitized points was used to obtain both a continuous depiction of the body posture and the total body length extended out of the burrow. Each recording session was divided into three to nine time intervals ('sections'), 3.5 min long each, in which the posture was digitized every 10 s. Three different eels were analyzed in each section, yielding 21 digitized postures per eel per section, or a total of 63 postures per section. Sections were selected based on the criterion that the eels are extended out of their burrow throughout the recording interval. That is, sections during which the eels retreated into their burrows were excluded from the analysis.

The current meter provided information on the current speed and direction. However, the determination of the orientation of the eel relative to the current direction was challenging, as the absolute orientation of each camera could not be recorded precisely. To overcome this problem, we were able to visually observe that the eel's lower body (up to ~ 20 cm above bottom) was always slanted directly down current. Accordingly, the current direction during each section was inferred based on the average slanting angle of the lower body segment (10–20 cm in length) for three eels per section ($N=63$). We validated this method using two approaches. (1) In two sessions, the heading of the current meter, clearly seen by the two cameras, was calculated from the 3D images, allowing the calculation of the average current direction from the instrument's records for each section. Comparison of this direction to the direction calculated based on the inclination of the eel's lower body yielded an estimate that deviated by 15.3 deg (Fig. S3A). (2) In three different weak-current sessions (<6.5 cm s^{-1}) we compared the eel's inclination with the orientation of a neutrally buoyant tape, 0.3 m in length, attached at one end to the top of a 0.2 m tall pole seen by the 3D cameras. As the tape was dragged by the flow, its orientation, digitized from the 3D images every 3.33 s, was used as a proxy for the current direction. This comparison yielded an estimate that deviated by 27.3 deg from that measured with the tape (Fig. S3B). Based on the above, we used the inclination of the eel's lower body as an indication of the current direction, considering the fact that this proxy deviated from the true direction by the aforementioned magnitudes. The effect of those deviations on our calculation of drag coefficient, drag force and torque (see below) in the range of current speeds observed in this study was small, ranging from 2.3 to 3.3%.

Throughout the text, the 3D reconstruction of the eels was rotated around the Z -axis so that the current direction is parallel to the Y -axis.

Biomechanics

Our goal was to calculate the drag coefficient (C_D), drag force (F_D) and the hydrodynamic torque (M) exerted on the eels by the flow as function of current speed and body posture. Our calculations were based on the assumption that the eels are exposed to laminar flow. This assumption was reasonable given the flat seabed and low current speeds of 3 to 30 cm s^{-1} (Reynolds numbers of 300 to 3000, respectively, using 1 cm as the diameter of the eels' cylindrical body and kinetic viscosity of 1.0×10^{-6} m 2 s^{-1}).

For the calculations, we applied a simplified finite element approach. The exposed eel length was divided into consecutive segments 2 cm long each. The above hydrodynamic parameters were calculated for each one of the segments separately and then summed over the entire body length. The diameter and the length of the eels were calculated using the 3D reconstruction of the video records; the diameter was determined at the beginning of the records, whereas the length of the eel was calculated separately in each frame (see above).

Note that throughout this study, our calculations of the above parameters did not consider the potential effects of the eel's elongated dorsal fin. Therefore, our study focuses on comparative analyses, assessing the relative effects of different postures and body lengths, rather than seeking absolute values.

Drag coefficient

The drag coefficient is a dimensionless parameter, representing the hydrodynamic properties of an object's shape. A more streamlined object will have a lower drag coefficient, implying a lower drag force for the same current speed and object area. To find the drag coefficient, we calculated the normal and the axial force coefficients (C_N and C_T , respectively) for a cylinder with its length inclined into the flow, and found the components parallel to the direction of the current as in Ellington (1991):

$$C_{D(n)} = \left[1.1 + \frac{22}{Re(d)} \right] \sin^3 \alpha_n + \left[\frac{1.33\pi}{\sqrt{Re(l)}} + \frac{2\pi(l/d)}{Re(l)} \right] \cos^3 \alpha_n, \quad (1)$$

for $\alpha_n < 90$ deg and:

$$C_{D(n)} = \left[1.1 + \frac{22}{Re(d)} \right] \sin^3 \alpha_n + \left[\frac{1.33\pi}{\sqrt{Re(l)}} + \frac{2\pi(l/d)}{Re(l)} \right] \cos^3 (180 - \alpha_n), \quad (2)$$

for $\alpha_n > 90$ deg, where $Re(d)$ and $Re(l)$ are the Reynolds numbers using the width and length of the eel (outside the burrow), respectively, as the representing lengths. The angle α is the eel's local angle of attack, defined as the angle between the direction of the flow and the orientation of the n th body segment in the vertical plane that is parallel to the flow (Fig. 2). The left term in Eqns 1 and 2 represents the drag coefficient owing to normal flow (C_N) and the right term is the drag coefficient owing to axial flow (C_T) of a slender cylinder.

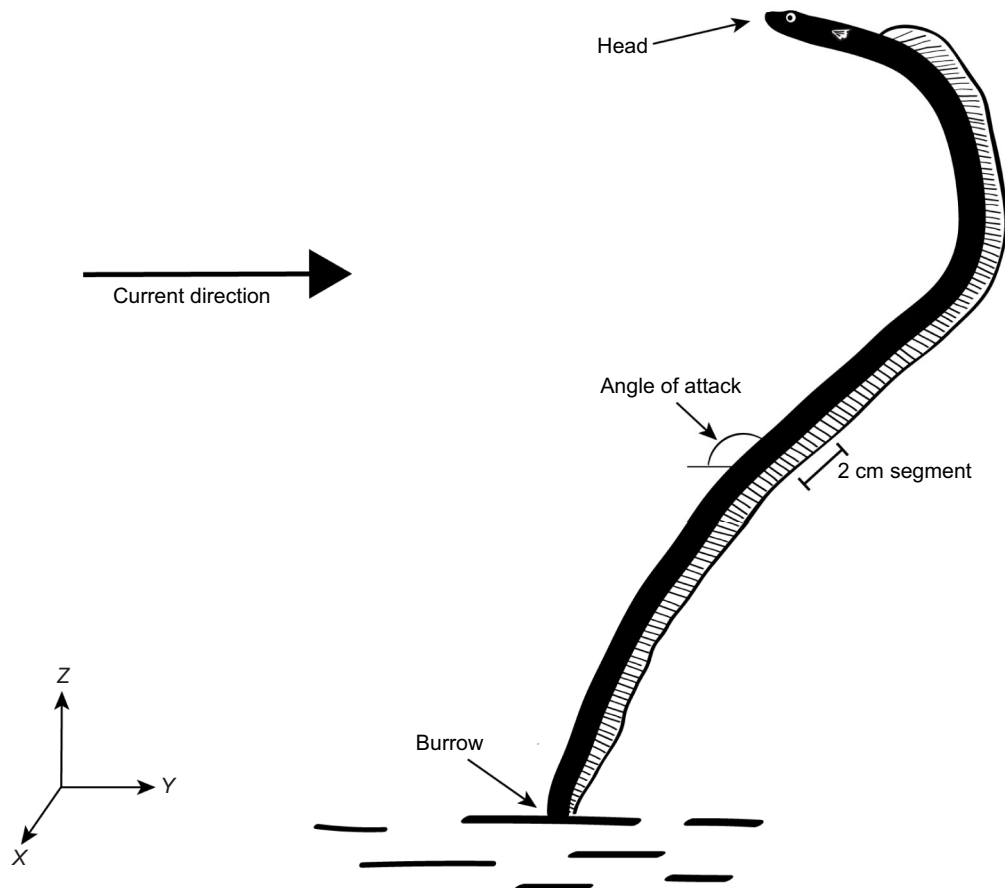


Fig. 2. Illustration of a garden eel in the YZ plane used for calculation of the hydrodynamic parameters. The Y-axis is parallel to the direction of the current and Z is the vertical axis. To calculate those parameters, the eel's extended body length was divided into 2-cm-long segments, and the angle of attack (α ; the angle of the eel's body towards the current) was calculated separately for each segment in the YZ plane.

In every frame digitized, the drag coefficient was calculated for each segment and then averaged for the eel's entire length extending above the burrow.

Drag force

The drag force applied by the flowing water on a body segment of the foraging garden eels is:

$$F_D = \frac{1}{2} C_D \rho A v^2, \quad (3)$$

where C_D is the drag coefficient of the segment, ρ is the density of the fluid (1028 kg m^{-3} for seawater; Reiss and Hottinger, 1984), A is the segment's area reference (segment length \times eel segment diameter, where the length of the segment is 2 cm and its diameter is the value measured by the 3D reconstruction of the eels) and v is the current speed.

The total drag force on the eel was the sum of F_D over the entire length of the eel (all segments), calculated for each digitized frame and averaged for the 3.5 min long section and then averaged over the three digitized eels, yielding the section's average F_D .

Hydrodynamic torque

To calculate the torque applied by the current on the eel at the opening of its burrow we found the cross product of the position vector between the burrow and a point on the eel's body and the

force vector at this point:

$$\mathbf{M}_b = \mathbf{r}_{bF} \times \mathbf{F}, \quad (4)$$

where \mathbf{M}_b is the moment in vector form, \mathbf{r}_{bF} is the position vector between the burrow and the point of force application and \mathbf{F} is the hydrodynamic force vector. This moment represents the torque a garden eel has to resist in order to avoid being passively bent backwards or even pulled out of the burrow by the current.

Note that the segment-specific torque was calculated using the segment's center as the point of reference. A sum of the torque values over the whole body length was used to calculate the torque applied on the eel at the opening of its burrow. Again, the torque values were calculated for each eel in each digitized frame and averaged over the 3.5 min section and then averaged over the three digitized eels, yielding the section's average torque.

Feeding rates

Direct determination of the *in situ* feeding rates of the garden eels was challenging. Therefore, we used visual records of strike rates as a proxy of feeding rate, assuming that all strikes were successful. Strikes were quantified by divers counting the number of strikes by individual eels during a 1 min interval for each eel. A total of 21 dives were performed, in which 10–30 eels were recorded per dive (Table S2). Current speed and zooplankton density were concurrently measured using a current profiler (Aquadopp 2 MHz, Nortek, Norway) and plankton net tows, respectively. Plankton tows

were performed using a 200 μm plankton net, 50 cm mouth diameter, either towed by a pair of divers or used as a stationary net, moored 30–50 cm above the bottom, up-current of the eel colony. Zooplankton in the samples was counted using a dissecting scope and converted to density based on simultaneous flow measurements.

Statistical analyses

All statistical parameters and tests (Pearson correlation and regression analyses) were performed using SYSTAT version 13 (Systat Software Inc., San Jose, CA, USA).

RESULTS

The garden eels we recorded ranged from 0.6 to 1.5 cm (mean of 1 cm) in body diameter, with 33–66 cm of body length extending out of the burrow (mean of 49 cm).

Current speed had a substantial effect on the posture of *G. sillneri* (Fig. 3). Under weak current conditions ($<5\text{ cm s}^{-1}$), the eels exhibited a nearly vertical posture with the head pointing towards the current (Fig. 3A), from which they occasionally curved their bodies in all directions in order to strike drifting prey. Curving was sometimes limited to the upper part of the body, apparently when the prey was close, and sometimes the entire body moved toward the prey. Complex postures, consisting of successive bending, were sometimes observed when a new strike was initiated while the bending posture of a previous strike still persisted. As current speed increased, the eels became more concave, with the upper half of the body bending more towards the current, while the lower part, close to the burrow, became more inclined down-current (Fig. 3B). Under strong current conditions ($>25\text{ cm s}^{-1}$), most of the body was curved, with only $\sim 5\text{ cm}$ of the extended lower body being inclined down-current (Fig. 3C). In addition to changing the posture, under strong current conditions, the eels also shortened the length of the extended part of their body, with a decrease from an average of 54.2 cm extension in weak currents (3 cm s^{-1}) to 41.3 cm in currents of 30 cm s^{-1} ($P<0.001$, $N=68$ sections based on 32 individuals; Fig. 4).

The eel's drag coefficient (C_D) decreased logarithmically as current speed increased ($R^2=0.85$, $N=68$, $P<0.00001$), from nearly 1.0 at 3.3 cm s^{-1} to 0.26 at 30 cm s^{-1} (Fig. 5). The total drag force exerted on

the eels increased by three orders of magnitude, from nearly $4.1\times 10^{-5}\text{ N}$ at a current speed of 3 cm s^{-1} to $5.31\times 10^{-2}\text{ N}$ at 30 cm s^{-1} , following a second-order polynomial curve ($R^2=0.92$, $N=68$, $P<0.00001$; Fig. 6A). Had the eels retained the posture typical for weak currents (3.3 cm s^{-1}) under conditions of stronger currents (30 cm s^{-1}), the drag force they would have experienced would be up to four times stronger (0.2 N). The observed decline in drag force, relative to that expected had the eels' posture remained unchanged, was due partially to the change in posture (Fig. 3) and partially to their slight retreat into the burrow (Fig. 4). A virtual simulation was used to examine the contribution of the latter (body shortening) by digitally shortening the virtual eel's segments by 20% ($N=3$ eels; under conditions of 3.3 cm s^{-1}), while keeping C_D constant (the effect of body shortening, without changing body width, on the C_D was 0.3%, i.e. negligible). This simulation indicated that as currents became stronger, the effect of changes in posture gradually became more dominant than that of body shortening, increasing from approximately 52% of the total effect at 13 cm s^{-1} to 74% at 30 cm s^{-1} (Fig. 6A).

The hydrodynamic torque exerted on the eels at the aperture of their burrows ranged from 4.8×10^{-4} to $1.0\times 10^{-2}\text{ Nm}$, increasing with current speed ($R^2=0.61$, $N=68$, $P<0.00001$; Fig. 6B). Under the hypothetical case, where the eels would have maintained the posture of the weak current (3.3 cm s^{-1}), the torque exerted at a current speed of 30 cm s^{-1} would have been 0.056 Nm, that is, 7.4 times greater compared with the observed torque (Fig. 6B).

The mean (\pm s.d.) feeding rate of garden eels was 18.8 ± 6.9 prey min^{-1} , increasing with current speed, prey density and, hence, prey flux (Fig. 7). A multiple linear regression analysis testing the correspondence between feeding rates and the two independent variables showed highly significant effects of current speed and prey density (Table 1). A simple linear regression analysis of feeding rate versus prey flux (a multiplication of prey density and current speed), indicated a highly significant correspondence ($R^2=0.67$, $P<0.0001$; Fig. 7C).

To assess the trade-off between food flux and drag of the exposed body, we also measured the 3D positions of the eel's head along the plane perpendicular to the flow direction. These measurements show that the standard deviation of the mean of those positions

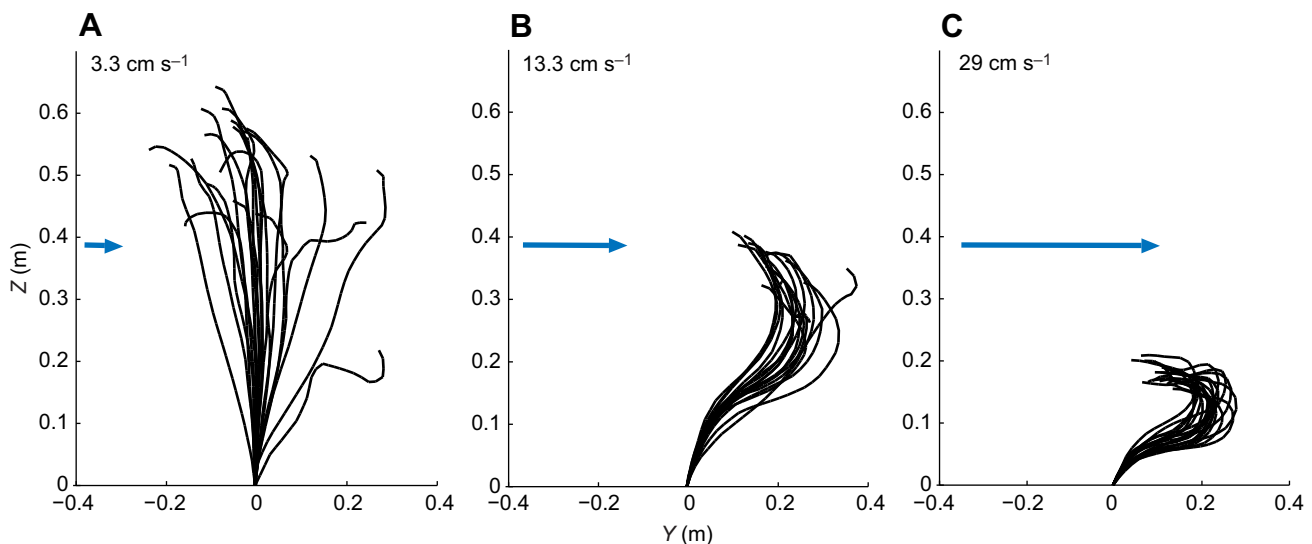


Fig. 3. Postures of three different eels under different current speeds. (A) 3.3 cm s^{-1} , (B) 13.3 cm s^{-1} and (C) 29 cm s^{-1} . The postures were obtained by reconstruction of the eel on the YZ plane (parallel to the current direction) once every 10 s during a section 3.5 min in length. Arrows indicate the current direction and magnitude. Each panel depicts different postures of the same eel.

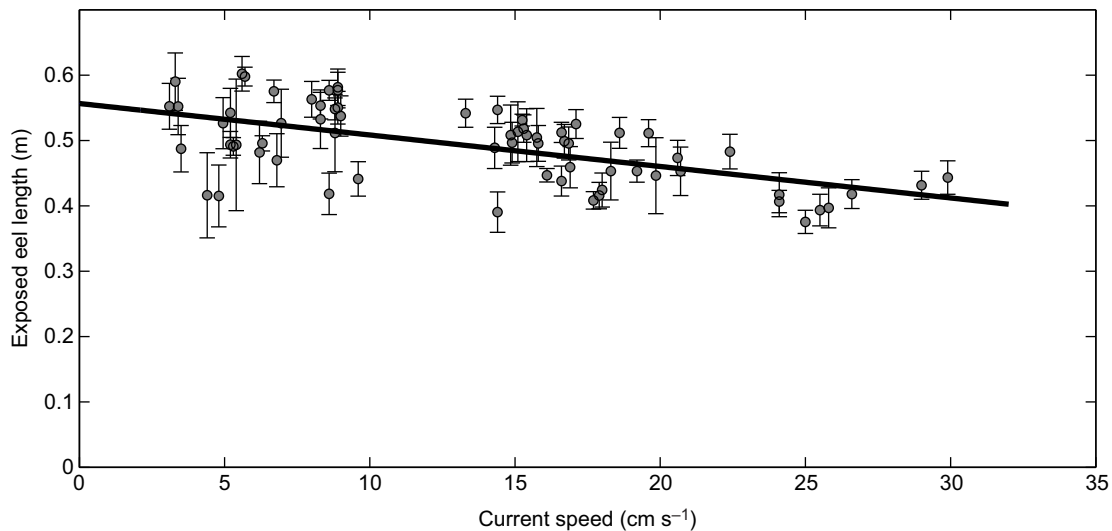


Fig. 4. Average length of the eel's body extended out of the burrow as function of current speed. Each data point indicates the mean length of three eels during a 3.5 min video section. Error bars indicate \pm s.d. among the three eels. The trendline indicates the linear fit to the data ($y=-0.004816x+0.5566$, $R^2=0.35$, $N=68$, $P<0.001$).

(Fig. S4) significantly declined with increasing flow speed (horizontal axis: Pearson correlation $R=-0.37$, $P<0.0001$, $N=66$; vertical axis: $R=-0.6$, $P<0.0001$, $N=67$). When those s.d. values are used as a proxy for the radius of the area across which the eel captures prey, a 3-fold decline in that area was observed when the current speed became six times stronger (from 5 to 30 cm s^{-1} ; Fig. S4). This flow-driven reduction in the eel's feeding cross-section area was corroborated by our direct measurements of the polygons depicted by the eel's head during intervals lasting 10 min [polygon area perpendicular to flow direction (cm^2)= $-5.57v+227$, Pearson correlation $R=-0.34$, $P<0.03$; $N=42$].

DISCUSSION

Many zooplanktivorous fish in coral reefs and other complex habitats (e.g. kelp forests) are site attached – foraging for drifting prey while holding position near shelters. Among that guild of fish,

garden eels are unique as they forage for zooplankton while being 'anchored' to the bottom. Although the 'sessility' of garden eels is not permanent, as individuals can switch locations (Fricke, 1970; Clark, 1980), their foraging is always performed while being anchored. This mode of foraging appears to alleviate the biomechanical constraint imposed by strong currents. In 'free' site-attached fish, such constraints cause a decrease in feeding efficiency with increasing flow speed (Kiflawi and Genin, 1997). When currents become stronger, free fish strike prey at progressively narrower angles relative to the flow direction, avoiding a situation in which their body will be oriented sideways to the flow. No such biomechanical limitation was observed in the present study, where a monotonous increase in feeding rate with increasing current speed occurred (Fig. 7A). In contrast, the eels' nearly linear functional response to changes in prey density was similar to that of 'free' zooplanktivorous fish (Fig. 7B).

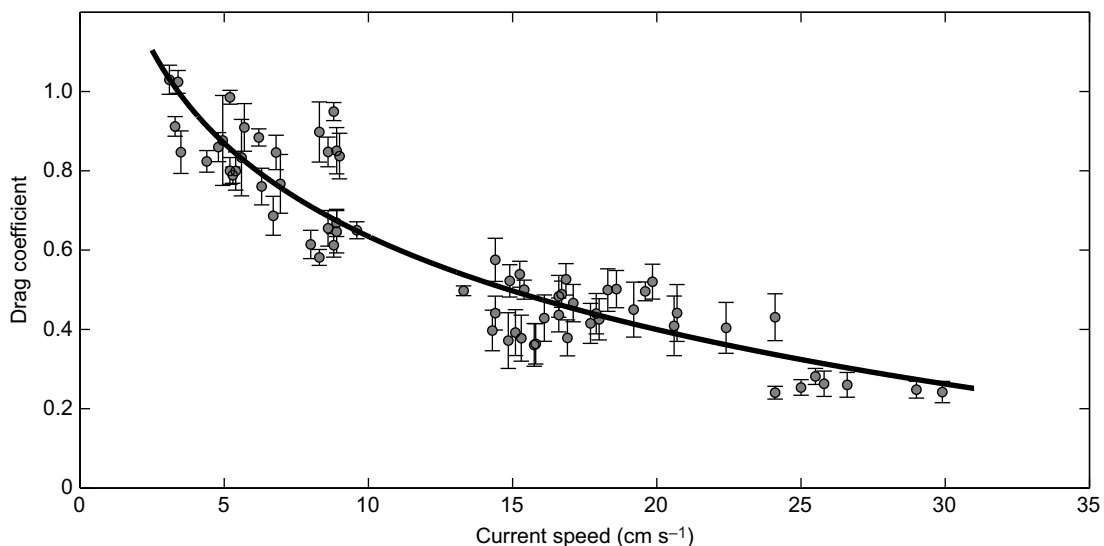


Fig. 5. Average drag coefficient as a function of current speed. Each data point indicates the mean calculated for three eels in a video section 3.5 min long (63 frames). Error bars indicate \pm s.d. among the three eels. The trend line indicates the logarithmic fit to the data [$y=-0.3389\log(x)+1.415$, $R^2=0.85$, $N=68$, $P<0.00001$].

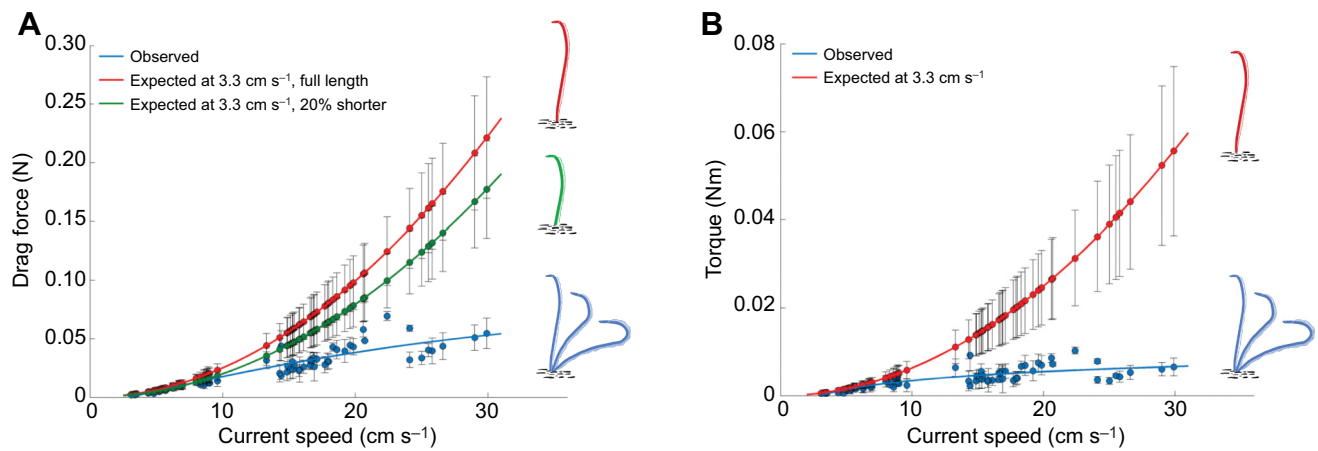


Fig. 6. The hydrodynamic force and torque exerted on the eels. (A) Total drag force exerted on the eels as a function of current speed. (B) Hydrodynamic torque at the opening of the burrow as a function of current speed. The observed data (change of posture and extended body length outside the burrow) are indicated in blue, where the corresponding equations describing the relationships are: drag force: $y = -2.867 \times 10^{-5}x^2 + 0.002915x - 0.008528$, $R^2 = 0.83$, $N = 68$, $P < 0.00001$; torque: $y = 0.002897 \times \log(x) - 0.0032$, $R^2 = 0.61$, $N = 68$, $P < 0.00001$. The expected values if the eels were to retain the posture observed at weak current (3.3 cm s^{-1} ; mostly upright and highly variable) are indicated in red, with the corresponding equations of drag force: $y = 2.457 \times 10^{-4}x^2 + 6.011 \times 10^{-5}x - 1.022 \times 10^{-5}$, and torque: $y = 6.168 \times 10^{-5}x^2 + 1.592 \times 10^{-5}x - 3.779 \times 10^{-6}$. The expected drag force exerted on an eel that retains its weak current posture (3.3 cm s^{-1}) with a 20% body shortening is indicated in green, with the following equation: $y = 1.966 \times 10^{-4}x^2 + 7.772 \times 10^{-5}x - 2.721 \times 10^{-6}$. Each data point indicates the mean calculated for three eels in a section of 3.5 min (63 digitized frames). Error bars indicate the standard deviation among the three eels. The drawings of the eels on the right side of each panel indicate the typical postures and lengths of the eels exhibited under conditions of 3 cm s^{-1} (red), under 3 cm s^{-1} but with body length shortened by 20% (green), and as naturally observed *in situ* (blue) under 3, 15 and 30 cm s^{-1} currents.

To utilize the advantage of higher prey fluxes under enhanced currents, the garden eels need to overcome the drag forces imposed by strong flows. Similar to sessile soft-bodied invertebrates (Koehl, 1977), garden eels modulate their body posture and length as a function of current speed (Figs 3 and 4), leading to substantial reductions in drag force and torque (Fig. 6). Under strong currents, all eels are uniformly orientated onto the current exhibiting strongly

curved body, whereas under weak currents high variation of orientations and postures are found among neighboring eels (Fig. 1).

Both the posture and the length of the extended body outside the burrow contribute to the reduction of drag force and hydrodynamic torque (Fig. 6). However, the change in posture is dominant in reducing the drag force under strong currents. By curving their bodies when currents are strong, the eels change the angle of attack

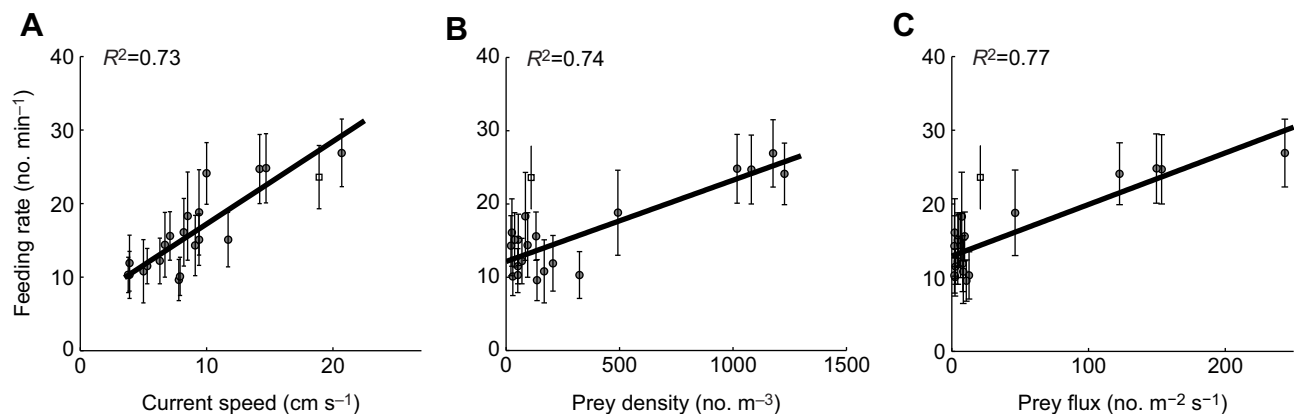


Fig. 7. Feeding rate of the eels as a function of prey availability. Feeding rate as function of (A) current speed, (B) prey density and (C) prey flux. Feeding rates refer to *in situ* strike rates, counted underwater (see Materials and Methods). Each data point indicates the mean calculated for at least 10 eels in a single dive. Error bars indicate the standard deviation of the feeding rates of individual eels counted in each of the ~ 20 min intervals (see Materials and Methods). Trend lines and R^2 values indicated on the plots are based on linear regression analysis. An outlier (open square), obtained during exceptional conditions of low prey density and strong current, was excluded from this regression analysis. When the outlier is included in the analysis, the corresponding R^2 values are 0.74, 0.61 and 0.67 for the data in A, B and C, respectively ($N = 21$).

Table 1. Multiple linear regression of feeding rate versus current speed and prey density

Effect	Coefficient	s.e.	Significance
Constant	7.47758	1.08648	***
Current speed (cm s ⁻¹)	74.09402	12.61685	***
Prey density (no. m ⁻³)	0.00589	0.00140	***

*** $P < 0.001$ ($N = 21$; all data points).

(Fig. 3), and thereby a longer part of the eel's body is oriented parallel, rather than perpendicular, to the flow. This change reduces substantially the drag coefficient of the eel's body (4-fold decrease as flow speed increases from 3 to 30 cm s⁻¹; Fig. 5). In turn, the lower C_D of the curved body causes a corresponding decrease in drag force, compared with a hypothetical state under which the eel retains the upright posture typical for weak currents (Fig. 6A). The contribution of higher Reynolds numbers under strong currents to the lowering of C_D was negligible compared with that of the posture change (a deviation of ~ 0.02 in the average C_D values was calculated under fixed values of Re of either 300 or 3000, corresponding to flow speed of 3 and 30 cm s⁻¹, respectively). Hence, the reduction in drag force is mostly attributed to the body curving (Fig. 3).

In addition, when currents intensified, the garden eels shortened the part of their body that remained outside the burrow by approximately 0.5 cm for each increment of 1 cm s⁻¹ increase in flow speed (Fig. 4). For example, for a body extension of 55 cm at 3 cm s⁻¹, the exposed part becomes shorter by approximately 24% by 30 cm s⁻¹. Although this shortening is beneficial as it reduces drag force, it also reduces prey encounter, as both prey density (Holzman et al., 2005; Yahel et al., 2005) and current speed (Vogel, 1994), and hence prey flux, decrease toward the bottom. Therefore, under weak current conditions, when hydrodynamic forces exerted on the eel are relatively small and prey flux is low, an upright, long posture provides a greater reach to capture prey. Although drag reduction is a linear function of body shortening, the ensuing

reduction in foraging volume is a cubic function of length reduction. For example, a 20% reduction in body extension reduces a hemispherical foraging volume by 49%. Conversely, under strong currents, the shortening-driven loss in foraging volume is partially counterbalanced by higher prey flux. For example, when the current speed increases from 5 to 30 cm s⁻¹, prey flux increases by 6-fold, whereas the observed decline in the cross-sectional area of the eel's foraging volume was only 4-fold (Fig. S4). Consequently, unlike 'free' zooplanktivorous fish, the eels' feeding rates monotonically increase with current speed (Fig. 7) throughout the range covered in our study (3–21 cm s⁻¹).

When currents become stronger, an eel wishing to maintain a relatively low drag force could potentially use an upright posture with a substantial shortening of the exposed body. Alternatively, the eel could curve its body without retreating very far into the burrow. Clearly, the eels prefer the latter approach, as under strong currents (> 20 cm s⁻¹) the curved posture allows the eel to maintain the same drag force with its head positioned ~ 7.5 cm ($\sim 60\%$) higher above the bottom compared with an upright posture (Fig. 8). No such difference was found under weak currents (< 10 cm s⁻¹; Fig. 8). Indeed, the eels were rarely curved when the currents were weak. An additional advantage of the curved body is the added potential for capturing prey that drifts far away from the eel (with no need to emerge out of the burrow). This difference is remarkable as, for example, under a flow speed of 30 cm s⁻¹, the predicted body length for the upright posture is 9 cm (red line in Fig. 8), whereas the observed value was nearly 41.3 cm (Fig. 4).

By modulating their posture and exposed body, the eels manage to maintain low torque (mean \pm s.d. = 0.004 ± 0.0025 Nm) over the range of 3 to 30 cm s⁻¹ flows. Had body curving not been used, the torque would have been up to 7.4 times higher (Fig. 6B), requiring higher energetic expenditure to maintain their posture.

Fluid motions greatly modulate the shape and posture of many marine sessile organisms. For example, the kelp *Nereocystis luetkana* and the macroalga *Chondrus crispus* reduce drag in strong currents using their high flexibility, allowing winding and

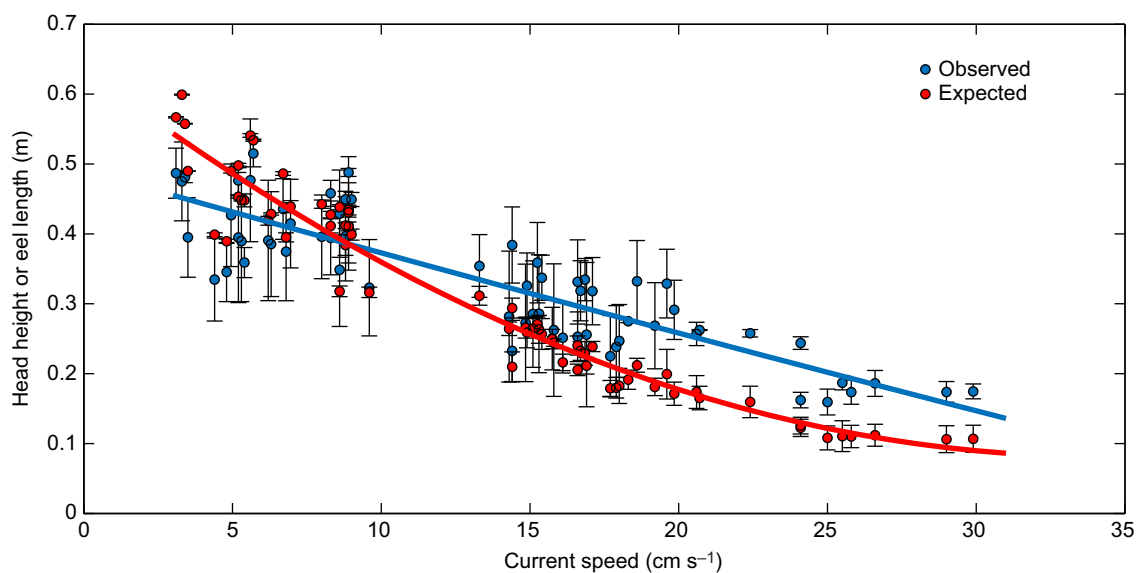


Fig. 8. Comparison between the observed height of the eels' head above bottom (blue) compared with the expected length of a nearly upright eel that would produce an equivalent drag force (red). The latter was calculated by considering a typical posture of an eel at 3.3 cm s⁻¹. The polynomial regression lines are: $y_{\text{obs}} = 1.787 \times 10^{-5}x^2 - 0.01201x + 0.4911$ ($R^2 = 0.76$, $N = 68$) and $y_{\text{exp}} = 0.0004736x^2 - 0.03244x + 0.6367$ ($R^2 = 0.94$, $N = 68$). Each data point indicates the mean of three eels in a video section 3.5 min long. Error bars indicate the standard deviation among the three eels.

bending with the flow (Koehl and Wainwright, 1977; Boller and Carrington, 2006). Sea pens rotate with the flow using a joint near their base, thereby decreasing drag force (Best, 1988; Vogel, 1994). Some sea anemones reduce drag forces by reconfiguring or retracting their tentacles that are orientated normal to the flow direction, while other species change their height by contraction (Koehl, 1977). On land, trees can be considered highly effective in reducing drag forces by changing the orientation of their branches and leaves (e.g. Vogel, 1989, 1994; Miller et al., 2012). Vogel (1984) suggested the use of the parameter E , indicating the degree of body re-configuration under strong currents, allowing a comparison between different taxa. E is the slope of the linear regression between the speed-specific drag (F_D/v^2) versus current speed (v) in a log–log plot. Negative values indicate reconfigurations that reduce drag force as flow speed increases. The value of E for the garden eels was -0.59 , quite moderate compared with that of the range of marine sessile animals and substantially smaller than that of exposed kelp fronds and trees (table 6.1 in Vogel, 1994). Yet, most of the organisms reported by Vogel (1994) passively respond to the fluid motion, mostly by bending or stretching downcurrent or downwind, whereas garden eels determine their posture actively, through behavior. In that regard, the sea anemones *Metridium* and *Anthopleura*, which actively control their tentacle reconfiguration and body stretching under strong currents (Koehl, 1977), are the only other sessile animals we are aware of in which active determination of body length was found.

Note that in this study we have calculated the expected drag forces, without directly measuring them. Deviations between real values and those calculated based on an assumption of smooth, cylindrical shape can occur as a result of many factors, including mucus coating (Hoyt, 1975), surface roughness and effects of fins (Vogel, 1994). Measuring those factors is beyond the scope of this study. Note, however, that our conclusions are based on relative, rather than absolute values, e.g. a comparison of drag force between different postures of the same body. Hence, we trust that our conclusions should remain valid when direct measurements of drag force and torque are made.

Marine habitats such as coral reefs and kelp forests, where shelters are readily available and currents continuously replenish water-borne, planktonic food, provide suitable conditions for a distinctive feeding mode among zooplanktivorous fish: quasi-stationary foraging close to a shelter, be it a coral, rock or another complex object. Indeed ‘free’ site-attached fishes flourish in shelter-rich coral reefs and kelp forests (Hobson and Chess, 1976; Hamner et al., 1988). Exposed sandy bottoms, in contrast, provide no protruding shelters. The ability of garden eels to construct their own shelter in the sand and at the same time effectively reduce drag forces in order to emerge from the burrow and feed in the flow allows them to be the only type of site-attached zooplanktivorous fish that occupies sandy bottoms in shallow, predation-rich habitats in the world’s oceans.

Acknowledgements

We are grateful to Hans Fricke for inspiring our work and for sharing with us his deep knowledge of the eels and their unique behavior. We thank Charlotte Wynn, Shir Bar and Yaela Reuben for their wonderful help with the challenging work in the field and laboratory. We are most grateful to the IUI staff for invaluable logistic assistance.

Competing interests

The authors declare no competing or financial interests.

Author contributions

Conceptualization: A.K., A.G.; Methodology: A.K., G.R., A.G.; Software: A.K.; Formal analysis: A.K., G.R., A.G.; Investigation: A.K., D.C., I.K.; Resources: G.R.,

A.G.; Writing - original draft: A.K., G.R., A.G.; Visualization: A.K.; Supervision: A.G.; Project administration: A.K., D.C., I.K.; Funding acquisition: A.G.

Funding

This research was funded by the Israel Science Foundation (grant 1211-14 to A.G.).

Supplementary information

Supplementary information available online at <http://jeb.biologists.org/lookup/doi/10.1242/jeb.179523.supplemental>

References

- Armstrong, S. L.** (1989). The behavior in flow of the morphologically variable seaweed *Hedophyllum sessile* (C. Ag.) Setchell. *Hydrobiologia* **183**, 115-122.
- Baynes, T. W. and Szmant, A. M.** (1989). Effect of current on the sessile benthic community structure of an artificial reef. *Bull. Mar. Sci.* **44**, 545-566.
- Bell, E. C. and Gosline, J. M.** (1997). Strategies for life in flow: tenacity, morphometry, and probability of dislodgment of two *Mytilus* species. *Mar. Ecol. Prog. Ser.* **159**, 197-208.
- Best, B. A.** (1988). Passive suspension feeding in a sea pen: effects of ambient flow on volume flow rate and filtering efficiency. *Biol. Bull.* **175**, 332-342.
- Böhle, J. E.** (1957). On the occurrence of garden eels in the western Atlantic, with a synopsis of the Heterocongrinae. *Proc. Acad. Nat. Sci. Philad.* **109**, 59-79.
- Boller, M. L. and Carrington, E.** (2006). The hydrodynamic effects of shape and size change during reconfiguration of a flexible macroalgae. *J. Exp. Biol.* **209**, 1894-1903.
- Carrington, E.** (1990). Drag and dislodgment of an intertidal macroalgae: consequences of morphological variation in *Mastocarpus papillatus* Kützinger. *J. Exp. Mar. Biol. Ecol.* **139**, 185-200.
- Chang, W.-L., Chi, K.-J., Fan, T.-Y. and Dai, C.-F.** (2007). Skeletal modification in response to flow during growth in colonies of the sea whip, *Junceella fragilis*. *J. Exp. Mar. Biol. Ecol.* **347**, 97-108.
- Clark, E.** (1980). Distribution, mobility, and behavior of the red sea garden eel. *Nat. Geogr. Soc. Res. Rep.* **13**, 177-186.
- Clark, E., Pohle, J. F. and Shen, D. C.** (1990). Ecology and population-dynamics of garden eels at Ras-Mohammed, Red-Sea. *Nat. Geo. Res.* **6**, 306-318.
- Denny, M. W. and Gaylord, B.** (2002). The mechanics of wave-swept algae. *J. Exp. Biol.* **205**, 1355-1362.
- Denny, M. W., Daniel, T. L. and Koehl, M. A. R.** (1985). Mechanical limits to size in wave-swept organisms. *Ecol. Monogr.* **55**, 69-102.
- Docker, M. F.** (ed.) (2014). *Lampreys: Biology, Conservation and Control*, Vol. 1. Dordrecht: Springer.
- Ellington, C. P.** (1991). Aerodynamics and the origin of insect flight. *Adv. Insect. Physiol.* **23**, 171-210.
- Fricke, H. W.** (1969). Biologie et compartement de *Gorgasia sillneri* (Klausewitz) et *Taenioconger hassi* (Klausewitz, Eibesfeldt) (Teleosteen) [Biology and behavior of *Gorgasia sillneri* (Klausewitz) and *Taenioconger hassi* (Klausewitz, Eibesfeldt) (Teleosteen)]. *CR Acad. Sc. Paris* **269**, 1678-1680.
- Fricke, H. W.** (1970). Ökologische und verhaltensbiologische Beobachtungen an den Röhrenaalen *Gorgasia sillneri* und *Taenioconger hassi* (Pisces, Apodes, Heterocongridae) [Ecological and behavioral observations of the garden eels *Gorgasia sillneri* and *Taenioconger hassi* (Pisces, Apodes, Heterocongridae)]. *Z. Tierpsychol.* **27**, 1076-1099.
- Fricke, H. W.** (1971). Zur Funktion, Morphologie und Histochemie der Schwanzdrüse bei Röhrenaalen (Pisces, Apodes, Heterocongridae) [On the function, morphology, and histochemistry of the tail gland in garden eels (Pisces, Apodes, Heterocongridae)]. *Mar. Biol.* **9**, 339-346.
- Gaylord, B. and Denny, M.** (1997). Flow and flexibility. I. Effects of size, shape and stiffness in determining wave forces on the stipitate kelps *Eisenia arborea* and *Pterygophora californica*. *J. Exp. Biol.* **200**, 3141-3164.
- Genin, A. and Paldor, N.** (1998). Changes in the circulation and current spectrum near the tip of the narrow, seasonally mixed Gulf of Elat. *Isr. J. Earth. Sci.* **47**, 87-92.
- Genin, A., Monismith, S. G., Reidenbach, M. A., Yahel, G. and Koseff, J. R.** (2009). Intense benthic grazing of phytoplankton in a coral reef. *Limnol. Oceanogr.* **54**, 938-951.
- Hamner, W. M., Jones, M. S., Carleton, J. H., Hauri, I. R. and Williams, D. M.** (1988). Zooplankton, planktivorous fish, and water currents on a windward reef face: Great Barrier Reef, Australia. *Bull. Mar. Sci.* **42**, 459-479.
- Harder, D. L., Speck, O., Hurd, C. L. and Speck, T.** (2004). Reconfiguration as a prerequisite for survival in highly unstable flow-dominated habitats. *J. Plant. Growth Regul.* **23**, 98-107.
- Harris, V.** (1990). *Sessile Animals of the Sea Shore*. London: Chapman and Hall.
- Hedrick, T. L.** (2008). Software techniques for two- and three-dimensional kinematic measurements of biological and biomimetic systems. *Bioinspir. Biomim.* **3**, 034001.
- Hobson, E. S. and Chess, J. R.** (1976). Trophic interactions among fishes and zooplankters near shore at Santa Catalina Island, California. *Fish. Bull.* **74**, 567-598.

- Holbrook, N. M., Denny, M. W. and Koehl, M. A. R.** (1991). Intertidal "trees": consequences of aggregation on the mechanical and photosynthetic properties of sea-palms *Postelsia palmaeformis* Ruprecht. *J. Exp. Mar. Biol. Ecol.* **146**, 39-67.
- Holzman, R., Reidenbach, M. A., Monismith, S. G., Koseff, J. R. and Genin, A.** (2005). Near-bottom depletion of zooplankton over a coral reef II: relationships with zooplankton swimming ability. *Coral Reefs* **24**, 87-94.
- Hoyt, J. W.** (1975). Hydrodynamic drag reduction due to fish slimes. In *Swimming and Flying in Nature*, Vol. 2 (ed. T. Y. T. Wu, C. J. Brokaw and C. Breman), pp. 653-672. New York: Plenum Press.
- Johnson, A. and Koehl, M. A. R.** (1994). Maintenance of dynamic strain similarity and environmental stress factor in different flow habitats: thallus allometry and material properties of a giant kelp. *J. Exp. Biol.* **195**, 381-410.
- Kiflawi, M. and Genin, A.** (1997). Prey flux manipulation and the feeding rates of reef-dwelling planktivorous fish. *Ecology* **78**, 1062-1077.
- Klausewitz, W.** (1962). *Gorgasia sillneri*, ein neuer Röhrenaal aus dem Roten Meer [*Gorgasia sillneri*, a new garden eel from the Red Sea]. *Senck. Biol.* **43**, 433-435.
- Koehl, M. A. R.** (1977). Effects of sea anemones on the flow forces they encounter. *J. Exp. Biol.* **69**, 87-105.
- Koehl, M. A. R.** (1982). The interaction of moving water and sessile organisms. *Sci. Am.* **247**, 124-134.
- Koehl, M. A. R. and Alberte, R. S.** (1988). Flow, flapping, and photosynthesis of *Nereocystis leutkeana*: a functional comparison of undulate and flat blade morphologies. *Mar. Biol.* **99**, 435-444.
- Koehl, M. A. R. and Wainwright, S. A.** (1977). Mechanical adaptations of a giant kelp. *Limnol. Oceanogr.* **22**, 1067-1071.
- Miller, L. A., Santhanakrishnan, A., Jones, S., Hamlet, C., Mertens, K. and Zhu, L.** (2012). Reconfiguration and the reduction of vortex-induced vibrations in broad leaves. *J. Exp. Biol.* **215**, 2716-2727.
- Monismith, S. G. and Genin, A.** (2004). Tides and sea level in the Gulf of Aqaba (Eilat). *J. Geophys. Res.* **109**, C04015.
- Okamura, B. and Partridge, J. C.** (1999). Suspension feeding adaptations to extreme flow environments in a marine bryozoan. *Biol. Bull.* **196**, 205-215.
- Reiss, Z. and Hottinger, L.** (1984). The Gulf of Aqaba (Eilat): ecological micropaleontology. Berlin, Heidelberg: Springer-Verlag.
- Sand-Jensen, K.** (2003). Drag and reconfiguration of freshwater macrophytes. *Freshw. Biol.* **48**, 271-283.
- Seymour, R. J., Tegner, M. J., Dayton, P. K. and Parnell, P. E.** (1989). Storm wave induced mortality of giant kelp, *Macrocystis pyrifera*, in southern California. *Estuar. Coast. Shelf. Sci.* **28**, 277-292.
- Stewart, H. L.** (2004). Hydrodynamic consequences of maintaining an upright posture by different magnitudes of stiffness and buoyancy in the tropical alga *Turbinaria ornata*. *J. Mar. Sys.* **49**, 157-167.
- Theriault, D. H., Fuller, N. W., Jackson, B. E., Bluhm, E., Evangelista, D., Wu, Z., Betke, M. and Hedrick, T. L.** (2014). A protocol and calibration method for accurate multi-camera field videography. *J. Exp. Biol.* **217**, 1843-1848.
- Tyler, J. C. and Smith, C. L.** (1992). Systematic significance of the burrow form of seven species of garden eels (Congridae: Heterocongrinae). *Am. Museum Novitates* **3037**, 1-13.
- Vogel, S.** (1984). Drag and flexibility in sessile organisms. *Am. Zool.* **24**, 37-44.
- Vogel, S.** (1989). Drag and reconfiguration of broad leaves in high winds. *J. Exp. Bot.* **40**, 941-948.
- Vogel, S.** (1994). *Life in Moving Fluids: the Physical Biology of Flow*. Princeton, NJ: Princeton University Press.
- Yahel, R., Yahel, G. and Genin, A.** (2002). Daily cycles of suspended sand at coral reefs: a biological control. *Limnol. Oceanogr.* **47**, 1071-1083.
- Yahel, R., Yahel, G. and Genin, A.** (2005). Near-bottom depletion of zooplankton over coral reefs: I: diurnal dynamics and size distribution. *Coral Reefs* **24**, 75-85.

Supplementary Information



Figure S1. An aerial photograph of the southern coast of Eilat, showing the two study sites (A and B). Light polygons indicate a permanent location of a colony. Yellow rectangles indicate locations of video records performed. Site A - offshore from the lighthouse ~0.4 km southwest of the Interuniversity Institute for Marine Sciences in Eilat. At this site the colony occupied a stretch of slope 6 m to 12 m in depth, 92 m in length. Site B - ~0.7 km N.NE of Taba border crossing. At this site the colony was found on a slope between 5 m – 15 m, 233 m in total length, quasi-separated to three sub-groups. The density of eels at Site A was about half that of Site B (1.75 ± 0.48 and 3.9 ± 0.57 individuals/m², respectively).

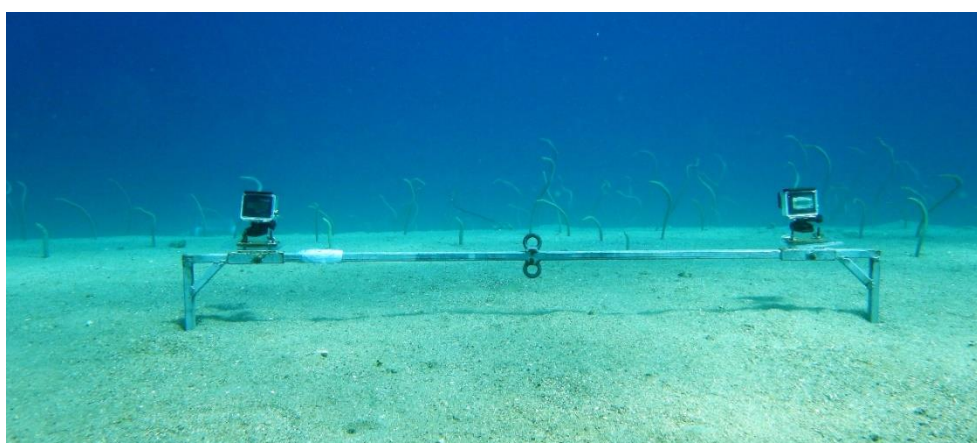


Figure S2. The underwater experimental setup. A stereo cameras system (two GoPro cameras, 2704x1524 pixels, 29.97 fps) for extracting three dimensional position data. The cameras were 1.8m apart, attached to a stand inserted in the sand. The cameras are directed towards a colony of garden eels at depth of 6 m.

Table S1: List of sessions recorded during the study and the sections within used

Date	Time	Location	Number of sections	Current speed range (cm/s)	
16/02/2016	06:25 – 07:22	Site A	4	3.3 – 7.0	
18/05/2016	15:40 – 16:44	Site B	8	3.5 – 9.6	
02/08/2016	08:29 – 09:26	Site A	4	5.4 – 24.1	*
09/08/2016	12:26 – 13:26	Site A	9	6.7 – 14.4	
22/08/2016	09:02 – 09:56	Site A	7	14.2 – 19.2	
23/08/2016	10:04 – 10:48	Site A	7	24.1 – 29.9	
05/09/2016	09:48 – 10:44	Site A	7	14.3 – 16.9	
21/09/2016	12:26 – 12:41	Site A	2	20.6 – 22.4	**
20/10/2016	10:59 – 11:55	Site A	10	14.9 – 19.9	
20/12/2016	13:49 – 14:44	Site B	8	3.1 – 9.0	
26/12/2016	07:59 – 08:55	Site B	2	4.8 – 8.6	

* Only two eels were analyzed in this session due to camera field of view limitations. The section with the current speed of 5.4 cm/s is shorter (01:07min) but was included in the analysis as it represents a significant change in the current speed during this session and allows examination of the same individuals at different current speeds.

** Shorter session was recorded due to camera failure.

Table S2: List of feeding rate experiments

Date	Time	Current Speed (cm/s)	Plankton Density (Prey/m³)	Number of eels examined
14/10/2014	11:30	9.4	492.7	10
19/10/2014	18:00	3.9	323.7	10
22/10/2014	07:50	10.0	1227.0	10
04/11/2014	14:10	7.8	136.4	10
12/11/2014	13:15	6.3	69.902	10
10/12/2014	11:20	20.7	1176.7	10
21/12/2014	10:55	5.0	168.2	10
23/12/2014	10:10	14.2	1080.8	10
31/12/2014	13:25	14.7	1018.2	10
04/07/2017	08:30	9.1	21.8	29
05/07/2017	07:00	8.5	85.5	32
06/07/2017	07:50	7.9	29.9	17
11/07/2017	18:00	8.2	25.9	31
12/07/2017	08:00	6.7	95.2	29
13/07/2017	08:00	3.9	206.8	30
18/07/2017	07:55	9.4	54.1	23
19/07/2017	07:55	18.9	110.6	31
20/07/2017	07:55	11.7	37.9	29
25/07/2017	08:20	7.1	132.0	10
26/07/2017	08:10	5.3	51.6	16
27/07/2017	07:50	3.8	51.7	13

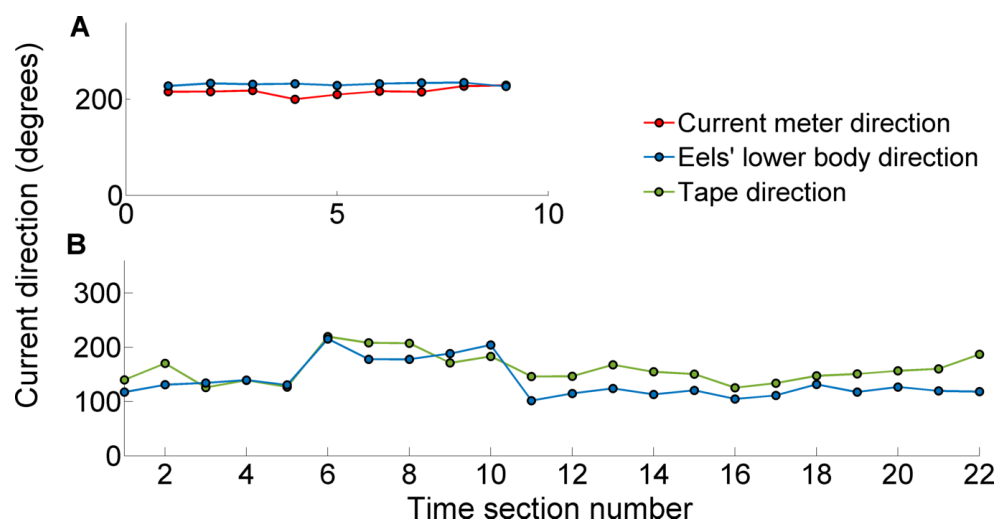


Figure S3. Comparison between the current direction calculated based on the inclination of the eel's lower body (10-20 cm from the burrow) and **(A)** current meter measurements under conditions of medium current speed (6.5-15 cm/s) and **(B)** measurements of the direction of a tape attached to a pole ~0.2 m above bottom for current speeds <6.5 cm/s. Each data point indicates the average direction of 3 individual eels each measured every 10 s during 3.5 min interval.

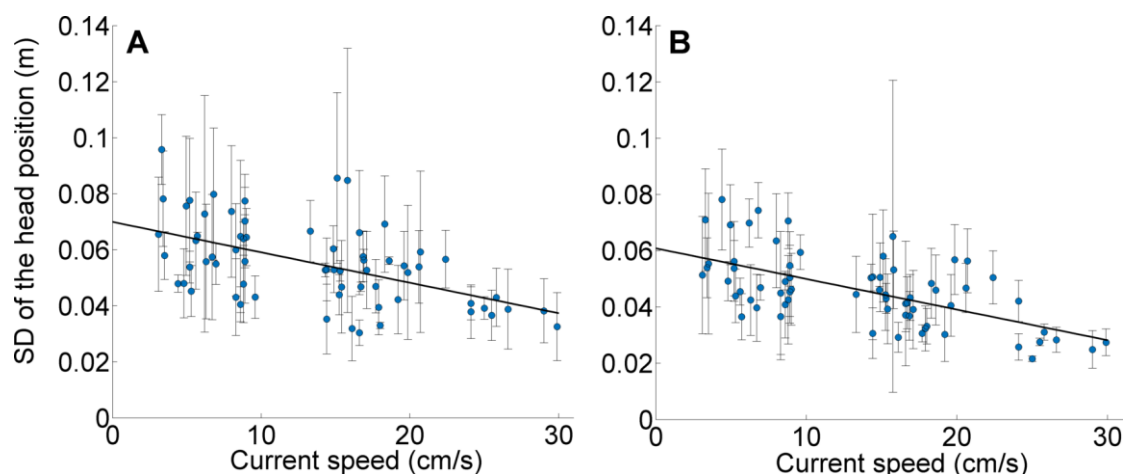
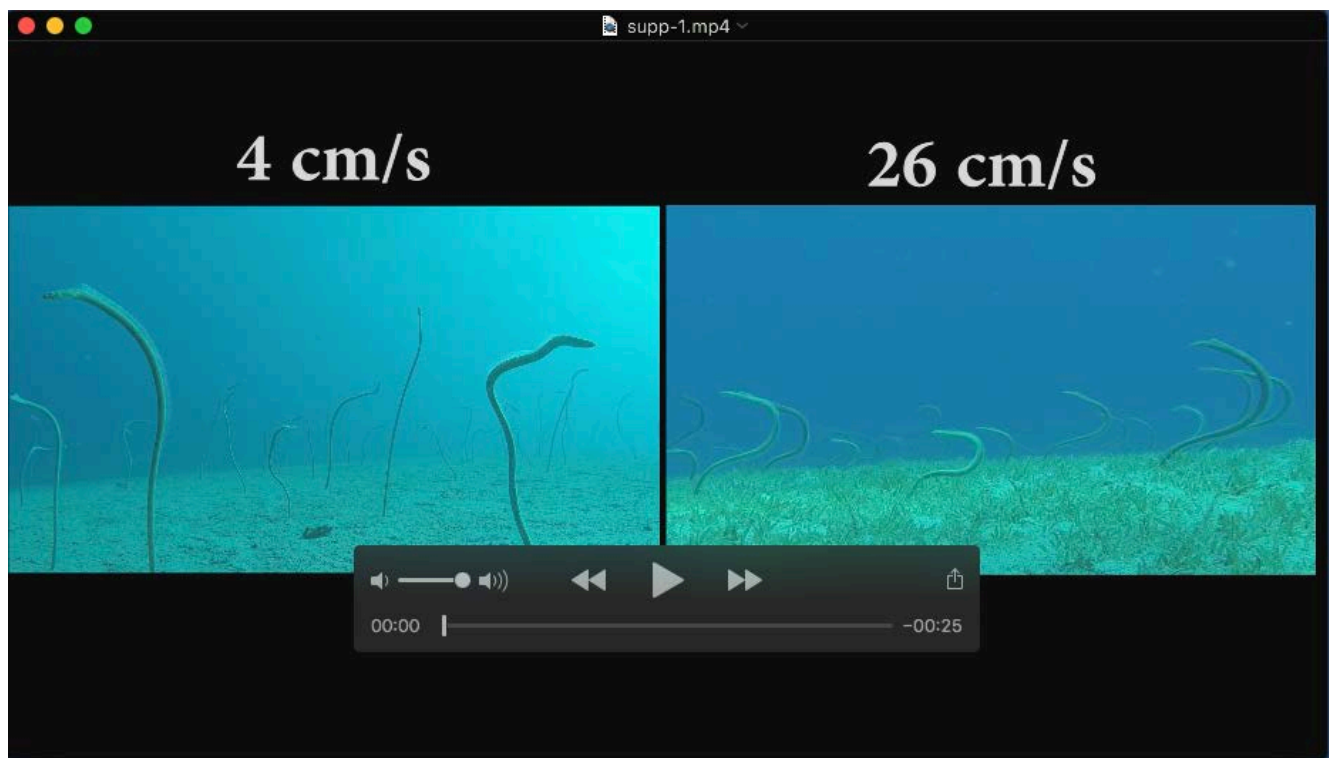


Figure S4. Standard deviation of the time varying position of the eels' head along: **(A)** horizontal axis perpendicular to the flow direction ($R^2=0.28$, $N=66$), and **(B)** vertical axis ($R^2=0.37$, $N=67$). Each data point indicates the average for the three eels in a section 3.5 min long. Error bars indicate the standard deviation among the three eels.



Movie 1. The flow-dependent changes in the feeding postures of the garden eel *Gorgasia sillneri*. A garden eel colony at 6 m depth in the northern Gulf of Eilat (Aqaba), Red Sea under condition of (left) weak current (4 cm/s) and (right) strong current (26 cm/s).